String Tension and Stability of Magic Tip-Suspended Nanowires

E. Tosatti,[1,2,3]* S. Prestipino,[1,2] S. Kostlmeier,[1,2] A. Dal Corso,[1,2] F. D. Di Tolla[1,2]

Multishell helical gold nanowires were recently imaged by electron microscopy. We show theoretically that the contact with the gold tips at either end of the wire plays a crucial role and that local minima in the string tension rather than the total wire free energy determine the nanowire stability. Density functional electronic structure calculations of the simplest and thinnest coaxial gold and silver wires of variable radius and chirality were carried out. We found a string tension minimum for a single-tube gold nanowire that is chiral and consists of seven strands, in striking agreement with observation. In contrast, no such minimum was found for silver, where the s-d competition leading to surface reconstruction is lacking.

Recent transmission electron microscope experiments have provided unprecedented detail about the structure and evolution of necks, bridges, and wires formed between gold tips (*1*–*4*). It was found that gold (110) nanobridges, which possess a regular crystalline face-centered cubic (fcc) structure when sufficiently thick (*1*) or short (*4*), can transform at diameters below ~15 Å into regular but noncrystalline wires several nanometers long, hanging between tips. These nanowires appear to form mostly discrete, multishell structures of specific "magic" sizes, and each tube consists of a triangular sheet folded cylindrically onto itself (*3*). These structures are exciting for many reasons. Wires represent a novel organization of matter, similar but not identical to clusters, which is yet to be fully understood (*5*). The structural transition from crystalline (fcc) to noncrystalline nanowires, including chiral ones for decreasing radius, confirms an earlier theoretical prediction (*6*). Nonetheless, the detailed stabilization mechanism leading to the observed chiral gold structures is unknown. Also, whereas nonequilibrium necks and their nanosecond evolution have been relatively well explored, particularly through simulation (*7*–*10*), the long-lived magic wires (which last for seconds at room temperature) are novel and not easily within the reach of simulation. The connection between thermodynamical, geometrical, mechanical, electronic, and ballistic conductance properties in these nanowires calls for a fresh approach.

The equilibrium state of an N-atom isolated cluster minimizes conventional free energy F (at zero temperature, this equals the total energy E). A free wire is a cluster of very large extension along one direction only and generally does not represent an equilibrium state because F can be lowered by transformation to a roughly spherical cluster, whose surface area is smaller by a factor of the order of $(9R/2L)^{1/3} \ll 1$, where L is the wire length and R is its radius [we will henceforth conventionally take the wire radius to be $R = (N/L\pi\rho)^{1/2}$, where N is the number of atoms and ρ is the bulk atom density]. However, our aim here is not to describe a free wire, but rather to describe a tip-suspended wire, that is, a long wire ($R \ll L$) in contact with bulk-like tips, with which it exchanges atoms. Imagine drawing a nanowire of constant radius R by pulling tips apart from length zero to L. If μ is the bulk chemical potential and F is the wire free energy, the positive work done in drawing the wire out of the tips is $(F - \mu N)$, or per unit wire length

$$f = \frac{F - \mu N}{L} \qquad (1)$$

f is a force that describes the generalized wire string tension that a tip-suspended wire will seek to minimize. To get a feel for this quantity, we can set roughly $F = \mu N + \gamma 2\pi RL$, where γ is a surface tension, leading to $f = 2\pi R\gamma$; the wire tension $f(R)$ generally increases with radius and has its absolute minimum at $R = 0$. The decrease in tension with shrinking radius is the driving force behind spontaneous wire thinning (*11*), which takes place by depletion of atoms from the nanowire to the tips, eventually leading to wire breaking. However, the tension $f(R)$ may also possess local minima, corresponding to favorable nanowire structures (Fig. 1). These minima signify long-lived metastable states, and we propose that they correspond to the magic observed nanowires. We thus explored a wide spectrum of free wire structures and calculated $f(R)$ for each, seeking the local minima. These minima should correspond to observed magic structures in all cases where an exchange of atoms between the nanowire and the tip is effectively realized within the time scale of the experiment.

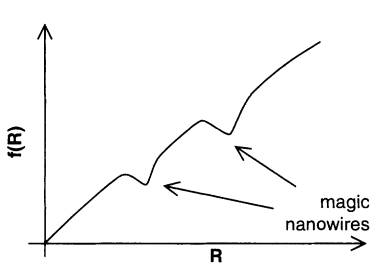

Fig. 1. String tension of a tip-suspended nanowire as a function of radius (schematic). Local minima signal long-lived magic nanowires. The wire disappears ($R = 0$) at true equilibrium.

For a first implementation of this method, we chose the thinnest and therefore simplest among the magic, noncrystalline gold nanowires observed in (*3*). According to Kondo and Takayanagi (*3*), magic nanowires consist of successive tubes, where each tube is formed by a triangular (111) lattice sheet that is folded onto itself to form a cylinder, similar to carbon nanotubes (*12*). The thinnest magic nanowire consists of a single tube and a central strand. We denote by (m, n) a tube consisting of m close-packed strands forming a maximal angle ranging from 30° ($n = 0$) to 0° ($n = m/2$) with the tube axis. As shown in Fig. 2, the tube unit cell is given by the vectors (orthogonal and parallel to the wire axis) $(ma_1 + na_2)$ and $(pa_1 + qa_2)$ with

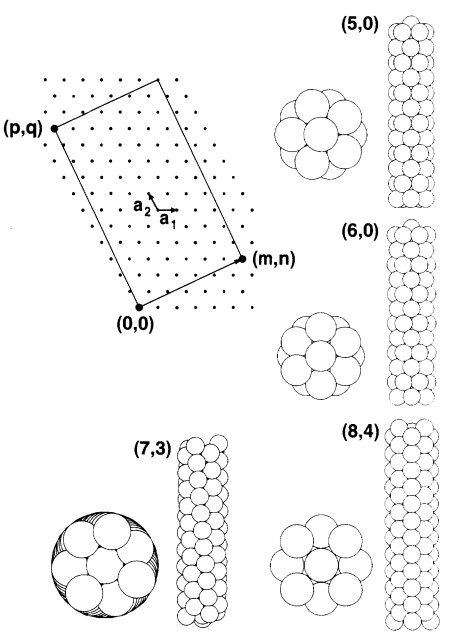

Fig. 2. Cylindrical folding of a triangular lattice for an (m, n) tube, with views of several coaxial tube nanowires. Each atom is pictured as a sphere of atomic radius. The (7, 3) gold nanowire (note its chirality) was reported to be magic in (*3*).

[1]International School for Advanced Studies (SISSA); [2]Istituto Nazionale di Fisica della Materia, Unità SISSA; [3]International Centre for Theoretical Physics, 34014 Trieste, Italy.

*To whom correspondence should be addressed. E-mail: tosatti@sissa.it

$q/p = (2m - n)/(m - 2n)$ and $n \leq m/2$. All tubes other than $(m, 0)$ and $(m, m/2)$ are chiral, and (m, n) and $(m, m - n)$ are mirror images of one another. At constant m, the wire radius, proportional to $(m^2 + n^2 - mn)^{1/2}$, shrinks for increasing n, as strands progressively align with the axis. The total atom number per cell is $N = 2(m^2 + n^2 - mn) + q$ (q atoms make up the central strand).

We considered infinitely long (m, n) nanowires (the effect of tips is included by Eq. 1) ranging from $(5, n)$ to $(10, n)$ and carried out the following protocol: (i) rough structural optimization with Lennard-Jones (LJ) potential; (ii) further structural refinement with a realistic embedded atom potential (*13*); (iii) full density functional calculation of electronic structure, total energy E, and string tension f (zero temperature); (iv) final structural refinement to minimize the calculated string tension; and (v) plotting the resulting optimal tension f against radius R and searching for magic nanowires as local minima of $f(R)$.

The result of this procedure for gold is shown in Fig. 3 (for each m value, only the largest and smallest n values are shown, for simplicity). The chiral (7, 3) nanowire ($m = 7$, $n = 3$; $p = 1$, $q = 11$; $L = 28.54$ Å; $N = 85$; $R = 3.92$ Å; and the actual tube radius is 2.78 Å) (*14*) exhibits the lowest tension and should thus be magic. The agreement of this theoretical result with the smallest observed magic nanowire (*3*) suggests that this theory should be extendable to the thicker magic nanowires. It should be stressed that minimizing tension instead of energy is crucial. In the present case, E would be lowest for the (8, 4) wire (which is, moreover, unstable against a crystalline form marked "rhombic" in Fig. 3), whereas f is lower for the (7, 3) wire because of a smaller radius and larger length L [length is proportional to $(p^2 + q^2 - pq)^{1/2}$].

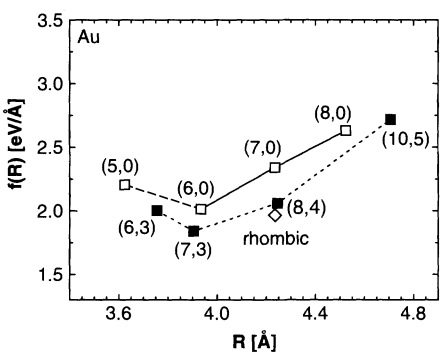

Fig. 3. Calculated (*22*) string tension (1 eV/Å = 1.6 nN) of tip-suspended gold nanowires at zero temperature (only the largest and smallest n values are shown). The minimum demonstrates why the (7, 3) nanowire is magic. The calculations were carried out for infinite tip-free wires, with structure relaxed to minimize string tension (Eq. 1), starting from initial wire geometries obtained by Voter's potential; μ(Au) = −4.401 eV was obtained from a separate bulk calculation.

Our approach also allows a full electronic characterization of the nanowires. The band structure may give important clues about the stability of magic wires, which could, for example, be connected to electronic shell closing, as in the case of sodium wires (*15*); the band structure also provides the number of conducting channels for ballistic transport. As Fig. 4 shows, there is no electronic shell closing in any of the (6, 0), (7, 3), and (8, 4) nanowires. The Fermi level is crossed by six, six, and eight conduction bands, respectively, as expected for cylindrical free-electron ("jellium") tubes of increasing radii. Moreover, all chiralities are equally metallic, unlike carbon nanotubes (*12*). We are thus left with the nontrivial task of uncovering the microscopic physical explanation for the stability of the magic nanowires.

We considered packing. For hard spheres, only $5 \leq m \leq 8$ may provide good contact. We find that the optimal LJ nanowire is in fact (5, 0), the same wire as B4, found in earlier simulations for aluminum (*6*) and a sort of analog of the 13-atom icosahedral cluster (*16*). Why does the gold wire include, in the outside shell, two more strands and become chiral on top of that? A clue may be surface reconstruction: the (111) topmost layer in fcc gold has a 4.5% higher lateral density (atom density on the tube) than all other layers (*17*). We find that the lateral density is 0.151 Å^{-2} for the (7, 3) wire, 2.9% higher than 0.147 Å^{-2} of the (6, 0) wire and 11.9% higher than 0.133 Å^{-2} of the (5, 0) wire. Thick, crystalline gold (110) nanowires have also been shown to reconstruct (*1*). It is thus tempting (*5*) to envisage the magic (7, 3) wire as the result of a kind of "wire reconstruction." Gold surface reconstruction (*17*) is related to s-d competition in bulk cohesion (*18*), where a large positive 6s Fermi pressure compensates a corresponding negative 5d pressure. At the surface, the 6s pressure can be released otherwise, for example, by relaxation of the first layer, leaving the 5d negative pressure uncompensated and free to force an increase of the lateral density. We tested whether this scenario is pertinent to the nanowires in two ways. First, we compared the calculated 6s Fermi energies of the three prototype wires [(6, 0), (7, 3), and (8, 4)] (Fig. 4) and obtained 9.12, 8.58, and 8.18 eV, respectively, indicating a clear decrease, as expected in the reconstruction picture. Second, we repeated the whole calculation protocol for another metal that does not reconstruct, namely silver (*18*). The (7, 3), (6, 0), (6, 3), and (5, 0) tensions are now indistinguishable in silver (Fig. 5), in line with expectations based on silver's weaker reconstruction tendency. In conclusion, both tests support the reconstruction mechanism behind the stabilization of the (7, 3) gold nanowire. It seems likely that this kind of physics will also be relevant to the thicker magic wires (*3*) not addressed here.

One last feature to be discussed is nanowire handedness and chirality. The possible occurrence of nanowire chirality was highlighted in earlier work (*6*), where, incidentally, a (7, 3) tube was first found by simulation (the inner tube of lead wire B7). In gold's (7,

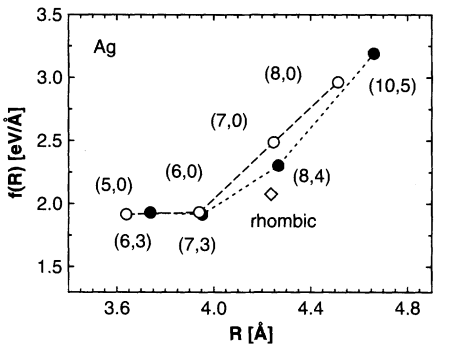

Fig. 5. String tension calculated for tip-suspended silver nanowires, using the same protocol as was used for gold (*22*); μ(Ag) = −3.402 eV. All wires from (5, 0) to (7, 3) are now degenerate, reflecting a reduced propensity to reconstruct and to yield a magic coaxial nanowire.

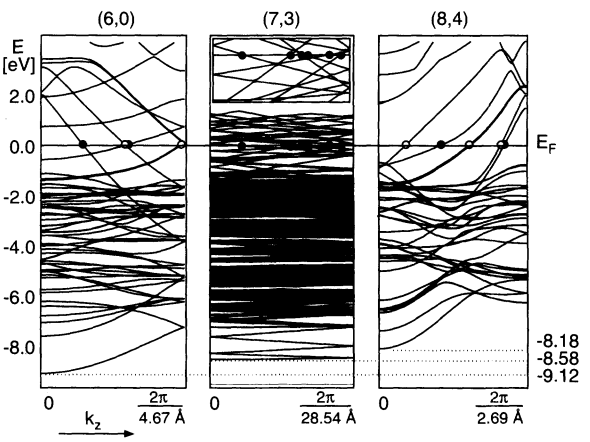

Fig. 4. Electronic structure of selected gold nanowires. There is full metallicity in each case, and the decreasing width of the 6s (or s and p) bands from (6, 0) to (7, 3) to (8, 4). Solid (open) circles mark single (doubly degenerate) Fermi crossings, indicating six, six, and eight conducting channels, respectively. Upper inset in the (7, 3) panel is a magnified detail of the bands crossing the Fermi level (the vertical scale is from −0.5 to 0.125 eV).

3) wire, chirality appears as a by-product of reconstruction (requiring a large number m = 7 of strands per tube) and of tight fitting of the central strand inside the tube, which requires that the radius $(m^2 + n^2 - mn)^{1/2}$ be minimized and thus that n be as high as possible (here, n = 3). It seems again likely that this mechanism could carry over to the thicker magic nanowires; because of high string tension, the wires with the largest n and with small R and large L values should again prevail. The largest n for odd m is $(m - 1)/2$, and this leads to chirality, in agreement with model structures presented for outer tubes with m = 11, 13, and 15 (*3*).

Experimental consequences of nanowire chirality should be interesting to pursue. Properties attributed to nanowire chirality were pointed out in (*19*) and (*20*). Direct calculation of the helical current density that is connected with each of the conducting channels of the (7, 3) wire, based on our wave functions, is possible. Whether the joint effect of all channels would be such as to yield a measurable inductance as in a kind of nanosolenoid (*21*) is an open question, presently under consideration.

References and Notes

1. Y. Kondo, K. Takayanagi, *Phys. Rev. Lett.* **79**, 3455 (1997).
2. H. Ohnishi, Y. Kondo, K. Takayanagi, *Nature* **395**, 780 (1998).
3. Y. Kondo, K. Takayanagi, *Science* **289**, 606 (2000).
4. V. Rodrigues, T. Fuhrer, D. Ugarte, *Phys. Rev. Lett.* **85**, 4124 (2000).
5. E. Tosatti, S. Prestipino, *Science* **289**, 561 (2000).
6. O. Gülseren, F. Ercolessi, E. Tosatti, *Phys. Rev. Lett.* **80**, 3775 (1998).
7. R. N. Barnett, U. Landman, *Nature* **387**, 788 (1997); U. Landman, *Phys. World* **11**, 18 (July 1998).
8. M. R. Soerensen, M. Brandbyge, K. W. Jacobsen, *Phys. Rev. B* **57**, 3283 (1998).
9. O. Tomagnini, F. Ercolessi, E. Tosatti, *Surf. Sci.* **287/288**, 1041 (1993); unpublished note.
10. G. Bilalbegovic, *Solid State Commun.* **115**, 73 (2000).
11. J. A. Torres *et al*, *Surf. Sci.* **426**, L441 (1999).
12. N. Hamada, S. Sawada, A. Oshiyama, *Phys. Rev. Lett.* **68**, 1579 (1992).
13. A. F. Voter, *Technical Report No. LA-UR-93-3901* (Los Alamos National Laboratory, Los Alamos, NM, 1987).
14. Coordinates of the (7, 3) nanowire are available at www.sciencemag.org/cgi/content/full/291/5502/288/DC1.
15. A. I. Yanson, I. K. Yanson, J. M. van Ruitenbeek, *Phys. Rev. Lett.* **84**, 5832 (2000).
16. F. C. Frank, *Proc. R. Soc. London Ser. A* **215**, 43 (1952).
17. E. Tosatti, F. Ercolessi, *Int. J. Mod. Phys. B* **5**, 413 (1991).
18. N. Takeuchi, C. T. Chan, K. M. Ho, *Phys. Rev. B* **40**, 1565 (1989).
19. V. N. Bogomolov, Yu. A. Kuzmerov, V. P. Petranovskii, A. V. Fokin, *Kristallografiya* **35**, 197 (1990).
20. T. G. Schaaff, R. L Whetten, *J. Phys. Chem. B* **104**, 2630 (2000).
21. Y. Miyamoto, A. Rubio, S. G. Louie, M. L. Cohen, *Phys. Rev. B* **60**, 13885 (1999).
22. In our density functional calculations, we used the local density approximation. Selected trials using a generalized gradient approximation (which we do not favor because it yields surface energies that are too low) gave similar results. For gold, we used plane waves and Vanderbilt ultrasoft pseudopotentials, as in work by A. Dal Corso *et al*. [*Phys. Rev. B* **56**, R11369 (1997)], and for silver, we used self-generated pseudopotentials [local s potential and core radii (in bohr), respectively, for 4d (1.8 and 2.4 ultrasoft radius) and for 5p (2.5)] derived as in work by G. Kresse and J. Hafner [*J. Phys. Condens. Matter* **6**, 8245 (1994)]. Kinetic energy cutoffs for wave functions and charge density is 25 and 200 rydbergs, respectively, for silver and gold. Spacing between one-dimensional k_z points is 0.147 Å^{-1} (k_z is the wave vector along the wire axis).

23. We acknowledge discussions and help from F. Ercolessi, K. Takayanagi, G. Santoro, G. Scoles, J. A. Torres, and A. Delin and support from Ministero dell'Università e della Ricerca Scientifica e Tecnologica (Cofinanziamento '99 and "Iniziativa trasversale calcolo parallelo"), Training and Mobility of Researchers (FULPROP), and Istituto Nazionale di Fisica della Materia.

2 October 2000; accepted 28 November 2000

Orbital Forcing of the Marine Isotope Stage 9 Interglacial

C. H. Stirling,[1,2]* T. M. Esat,[3] K. Lambeck,[3] M. T. McCulloch,[3] S. G. Blake,[3] D.-C. Lee,[1,2] A. N. Halliday[1,2]

Milankovitch orbital forcing theory has been used to assign time scales to many paleoclimate records. However, the validity of this theory remains uncertain, and independent sea-level chronologies used to test its applicability have been restricted largely to the past ~135,000 years. Here, we report U-series ages for coral reefs formed on Henderson Island during sea-level high-stands occurring at ~630,000 and ~330,000 years ago. These data are consistent with the hypothesis that interglacial climates are forced by Northern Hemisphere summer solar insolation centered at 65°N latitude, as predicted by Milankovitch theory.

Knowledge of the precise timing of past sea-level high-stands provides a crucial test of the Milankovitch model of climate change. This theory postulates that glacial-interglacial cycles are driven by periodic changes in July solar insolation at 65°N, caused by predictable variations in Earth's orbit (*1*). Previous U-series studies have focused almost exclusively on the last interglacial period, Marine Isotope Stage (MIS) 5.5, occurring at about 125,000 years ago (ka) (*2–9*). The timing of the MIS 5.5 sea-level high-stand appears consistent with Milankovitch forcing theory (*8, 10*). However, there is a growing body of evidence that factors other than 65°N summer solar insolation may have triggered the MIS 6-5 deglaciation, which appears to have begun before insolation started to increase (*10–12*). In contrast, the last deglaciation, which began at ~21 ka, can be adequately explained by 65°N insolation forcing alone. This raises the possibility that a different combination of forcing mechanisms may have operated during previous glacial-interglacial cycles (*13*).

To help resolve this apparent contradiction, the Milankovitch climate model can be tested by dating coral reefs that formed during older interglacials. However, it is exceedingly difficult to obtain reliable chronologic information for older sea-level high-stands because of a lack of well-preserved, datable coral.

Here, we report 30 precise U-series ages for a set of reef terraces formed during MIS 9 and MIS 15 on Henderson Island near Pitcairn Island in the equatorial Pacific (Fig. 1). These data, obtained using thermal ionization mass spectrometry (TIMS) (*7*) and multiple-collector ICP sector mass spectrometry (MC-ICPMS) (*14–16*), provide reliable and independent radiometric constraints on the global sea level curve at ~630 and ~330 ka.

Henderson Island is located in the extreme east of the Indo-Pacific subtropical province, resulting in severe restrictions in ecological development (*17, 18*). Therefore, coral terraces form only during exceptionally long (*18*) or warm interglacials. Offshore fringing reefs grew prolifically on Henderson Island during the MIS 9 interglacial, but no coral terraces appear to have formed subsequently during the MIS 7.1, MIS 5.5, or mid-Holocene sea-level high-stands.

Growth-position corals were collected from reef terraces along seven lyphenate cliff-section transects and one central fossil lagoon transect during the 1991–92 Pitcairn Islands Scientific Expedition (*18, 19*). U-series results for corals selected for dating are displayed in Web table 1 (*16*). In the 330 ka samples, ^{230}Th-age uncertainties (excluding the systematic contribution from the decay constants) can be smaller than ±2 ka, allowing the timing and duration of the MIS 9 interglacial to be well resolved. For completeness, all age uncertainties reported here include the decay constant contributions. Approximately one-third of the samples are

[1]Department of Geological Sciences, University of Michigan, Ann Arbor, Michigan 48109–1063, USA. [2]Institute for Isotope Geology and Mineral Resources, Department of Earth Sciences, ETH Zentrum, 8092 Zürich, Switzerland. [3]Research School of Earth Sciences, Australian National University, Canberra, ACT 0200, Australia.

*To whom correspondence should be addressed. E-mail: stirling@erdw.ethz.ch